Low-temperature high-density magneto-optical trapping of potassium using the open $4S \rightarrow 5P$ transition at 405 nm

D. C. McKay,[1,*] D. Jervis,[1] D. J. Fine,[1] J. W. Simpson-Porco,[1] G. J. A. Edge,[1] and J. H. Thywissen[1,2]
[1]*Department of Physics, CQIQC, and Institute for Optical Sciences, University of Toronto, M5S1A7 Canada*
[2]*Canadian Institute for Advanced Research, Toronto, Ontario, M5G 1Z8 Canada*
(Received 16 October 2011; published 21 December 2011)

We report the laser cooling and trapping of neutral potassium on an open transition. Fermionic ^{40}K is captured using a magneto-optical trap (MOT) on the closed $4S_{1/2} \rightarrow 4P_{3/2}$ transition at 767 nm and then transferred, with high efficiency, to a MOT on the open $4S_{1/2} \rightarrow 5P_{3/2}$ transition at 405 nm. Because the $5P_{3/2}$ state has a smaller linewidth than the $4P_{3/2}$ state, the Doppler limit is reduced from 145 μK to 24 μK, and we observe temperatures as low as 63(6) μK. The density of trapped atoms also increases, due to reduced temperature and reduced expulsive light forces. We measure a two-body loss coefficient of $\beta = 1.4(1) \times 10^{-10}$ cm^3/s near saturation intensity, and estimate an upper bound of 8×10^{-18} cm^2 for the ionization cross section of the $5P$ state at 405 nm. The combined temperature and density improvement in the 405 nm MOT is a twenty-fold increase in phase-space density over our 767 nm MOT, showing enhanced precooling for quantum gas experiments. A qualitatively similar enhancement is observed in a 405 nm MOT of bosonic ^{41}K.

DOI: 10.1103/PhysRevA.84.063420 PACS number(s): 37.10.De, 67.85.Lm, 32.80.−t, 34.50.Rk

I. INTRODUCTION

Magneto-optical trapping is a widely applied technique for creating cold, dense samples of neutral atoms. Ultracold-gas experiments typically use a MOT for accumulation and precooling, although laser cooling alone has been unable to create a quantum degenerate sample without a subsequent evaporative cooling step. Density in laser cooling is limited by repulsive radiation pressure due to reabsorption [1] and by collisional loss processes [2]. The temperature limit, in the simplest two-level theory, is the Doppler temperature, $k_B T_D = \hbar\Gamma/2$, where Γ is the linewidth of the excited state [3]. Fortuitously, the multilevel structure of ground states can allow for sub-Doppler temperatures [4,5], but these effects are not seen in all atomic species. Particularly, sub-Doppler cooling is nonexistent in ^{6}Li [6] and weak [7] or difficult to observe [8] in ^{40}K. Since these are the only two stable fermionic alkali-metal isotopes, and thus commonly used for the study of quantum degenerate Fermi gases, new cooling techniques would be beneficial.

Laser cooling on narrower lines can achieve lower temperatures, as has been demonstrated with alkaline-earth metals. In the case of ^{88}Sr [9], the broad 30 MHz cycling transition ($^1S_0 \rightarrow {}^1P_1$) at 461 nm is used to capture atoms, followed by cooling on the narrow 7.5 kHz forbidden transition ($^1S_0 \rightarrow {}^3P_1$) at 689 nm. This two-step process combines a large capture rate during the first stage with the low Doppler temperature of the second stage.

Alkali metals do not have forbidden cycling transitions; however, higher excited states do have smaller linewidths. In this work we excite potassium to the $5P$ state, which has a linewidth of 1.19 MHz, roughly five times smaller than the 6.04 MHz linewidth of the $4P$ state that has been used in all potassium laser-cooling experiments to date. In addition to reduced Doppler temperatures, higher-state transitions may provide other advantages: multiphoton decay channels allow for background-free detection, and the smaller transition wavelength reduces the diffraction limit of imaging and manipulation. A specific advantage of the potassium $4S \rightarrow 5P$ transition near 405 nm is the availability of inexpensive GaN diode lasers in the 395–410 nm range. One disadvantage of higher-state transitions in alkali metals is that they are open transitions. After excitation from the $4S_{1/2}, F = 9/2$ ground state to the $5P_{3/2}, F' = 11/2$ excited state, ^{40}K can decay via a three-photon cascade to the $F = 7/2$ ground state, which cannot be excited by the same laser-cooling light. Furthermore, the cascade decay acts to depolarize the atomic gas. Both of these effects can interrupt laser-cooling mechanisms.

It has been shown in a variety of systems that laser cooling is possible both with cascading and with open transitions. Examples include metastable noble gases [10], lanthanides [11], excited-state alkali metals [12], ground-state alkali metals [13], and molecules [14]. Similar to our work, the cooling of He* [10] and ^{6}Li [13] use the transition from the nS ground state to the $(n+1)P$ excited state. In the case of He*, a MOT on the $2S \rightarrow 3P$ transition at 389 nm, which is cascading but closed, was shown to have a lower two-body loss rate β, lower reabsorption rates, and a larger cooling force per recoil, resulting in increased density. No reduction in temperature was seen since the He* $2P$ and $3P$ excited states have the same lifetime. In the case of ^{6}Li, a MOT on the open $2S \rightarrow 3P$ transition at 323 nm did have a reduced temperature, but not an increased density. Unlike lithium and metastable helium, potassium has a D-state decay channel that could perturb laser cooling more significantly (see Fig. 1).

In this work, we explore cooling and trapping on the "blue" $4S_{1/2} \rightarrow 5P_{3/2}$ transition of ^{40}K at 405 nm. Atoms are first accumulated in a standard MOT on the "$D2$" $4S_{1/2} \rightarrow 4P_{3/2}$

*Current address: Department of Physics, University of Illinois, Urbana, Illinois 61801, USA.

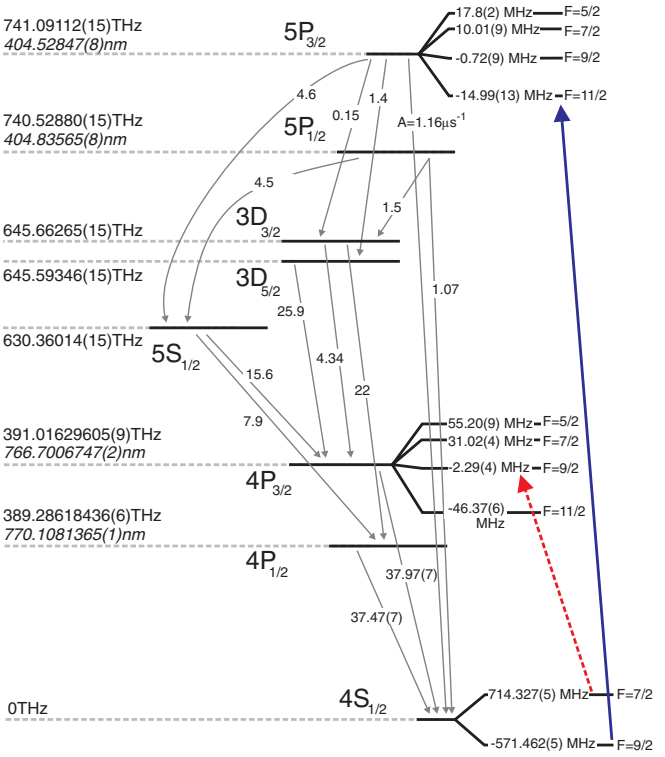

FIG. 1. (Color online) Level diagram including all the possible decay channels of the $4S \rightarrow 5P$ transition in ^{40}K. Transition probabilities are from [15] and listed as $A = 1/\tau$ in units of μs^{-1}. Except for $4P \rightarrow 4S$ (from [16]), the uncertainties in transition probability rates are not shown explicitly. The uncertainties in the $5P \rightarrow 4S$ rates are less than 8%, but all other rates are estimated to have uncertainties between 25% and 50%. The total measured lifetime from all decay channels is 134(2) ns for $5P_{3/2}$ [17] and 137.6(1.3) ns for $5P_{1/2}$ [18]. Level energies E referenced from the $4S$ state are from [15] and presented in both frequency units (as E/h) and wavelength units (in italics, as hc/E). Hyperfine splittings ΔE referenced to the level energies are from [19] for $4S_{1/2}$ and $5P_{3/2}$, from [15] for $4P_{3/2}$, and given in frequency units (as $\Delta E/h$). The solid blue and dashed red arrows indicate the cooling and repump hyperfine transitions, respectively, used for laser cooling.

transition at 767 nm, for which the capture rate is high. The cloud is then transferred to a blue MOT, where we observe a three-fold reduction in temperature and a ten-fold increase in density. Although the capture velocity and beam size of the blue MOT are small, we observe almost perfect transfer between MOTs. We find that loss rates in the blue MOT from two-body loss and photoionization are higher than in the $D2$ MOT, but these processes play little role on the sub-100 ms timescale that we observe is necessary for equilibration.

II. $4S_{1/2} \rightarrow 5P_{3/2}$ TRANSITION: THEORY AND BACKGROUND

Figure 1 shows a level diagram of potassium including all possible decay paths from the $5P_{3/2}$ state. The transition probability for $4S_{1/2} \rightarrow 5P_{3/2}$ is $2\pi \times 185$ kHz, thirty times weaker than the $2\pi \times 6.04$ MHz $D2$ transition. However, the excited state is broadened to $\Gamma = 2\pi \times 1.19$ MHz by other decay channels: five out of six times the $5P_{3/2}$ state decays via a three-photon cascade instead of emitting a single blue photon.

TABLE I. Key excitation properties of the $4S_{1/2} \rightarrow 5P_{3/2}$ transition, with the $4S_{1/2} \rightarrow 4P_{3/2}$ transition shown for comparison. Where relevant, the drive is assumed to be σ^+ polarized. Saturation intensity is defined as the drive strength at which 25% of the population is in the excited state. "Steady-state polarization" is the fraction of atoms in $F = 9/2$ that are in the $m_F = +9/2$ sublevel, with a drive at I_{sat}. "Depumping probability" is the percent decay from $|11/2, 11/2\rangle$ to the $F = 7/2$ manifold, through a multiphoton cascade. "Doppler temperature" is the steady-state temperature in the low-intensity limit and includes open-transition effects for $5P_{3/2}$.

	$4P_{3/2}$	$5P_{3/2}$
Linewidth $[\Gamma/(2\pi)]$	6.04(1) MHz	1.19(2) MHz
Branching ratio	Cycling	1/6.4(7)
Cross section (σ)	0.28 μm^2	0.010(1) μm^2
Saturation intensity (I_{sat})	1.752(3) mW/cm^2	23(2) mW/cm^2
Steady-state polarization	100%	61(1)%
Depumping probability	0%	18(2)%
Doppler temperature	145.0(3) μK	23.5(7) μK

We calculate excitation properties and cooling rates of the $4S \rightarrow 5P$ transition by finding the steady-state solution of the optical Bloch equation (OBE) that includes all relevant levels. Because the transition is not closed, continual excitation requires a repumping beam. As in the experiment, atoms are repumped on the $4S_{1/2}, F = 7/2 \rightarrow 4P_{3/2}, F = 9/2$ transition, whose strength is chosen here to be powerful enough that it is not the limiting timescale.

Table I summarizes key steady-state properties of excitation to the $4P$ and $5P$ states. Unlike in a cycling transition, the possibility of a multiphoton cascade prevents complete optical pumping. However, the depolarization effect is not quite as bad as Fig. 1 might suggest: 61% of atoms in the $F = 9/2$ manifold are in the doubly polarized $|9/2, 9/2\rangle$ state. The resonant scattering cross-section is nearly thirty times smaller than the $D2$ transition due to a narrow linewidth and smaller wavelength. This could be an advantage for cooling trapped or dense clouds since optical density is reduced. However, for the same reasons, the saturation intensity is an order-of-magnitude higher, increasing optical power requirements.

Laser cooling and trapping performance on the $4S \rightarrow 5P$ transition is estimated by including either Doppler or Zeeman shifts in the OBE calculation. The force on the atom is $\hbar\vec{k}$ times the calculated scattering rate, where $\vec{k}$ is the wave vector of each cooling beam. Close to zero velocity and position, atomic motion can be described as a simple harmonic oscillator, with oscillation frequency ω_0 and damping rate γ, plus a momentum diffusion term from recoil heating. Momentum diffusion is due to both absorption and emission along one of several possible decay paths. For each transition from state i to state j, the energy increase is $(\hbar k_{ij})^2/(2M)$, where $k_{ij} = \Delta E_{ij}/(\hbar c)$ and ΔE_{ij} is the energy difference between the states and M is the mass of ^{40}K. The total heating rate $\dot{E}$ gives rise to a steady-state temperature $\dot{E}/(\gamma k_B)$.

At comparable scaled detunings and saturations, Fig. 2(a) shows that the blue transition can achieve a higher cooling rate than the $D2$ transition. However, the maximum force and the

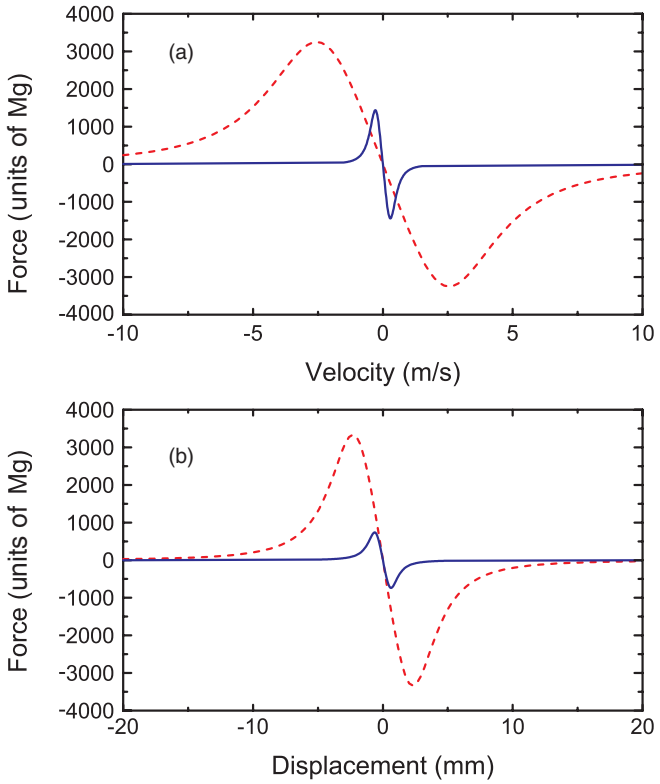

FIG. 2. (Color online) Blue cooling and trapping. Calculated force (in units of Mg, where g is gravitational acceleration) versus (a) velocity (at zero displacement) or (b) position (at zero velocity) for a 10 G/cm MOT at 767 nm (red dashed line) and 405 nm (blue dashed line). Both are calculated for counterpropagating beams at $-\Gamma/2$ detuning from resonance and with intensity per beam of $I_{\rm sat}/5$ where $I_{\rm sat}$ is indicated in Table I. For the 405 nm data there is a 767 nm repump beam on resonance with the $4S_{1/2}, F = 7/2 \rightarrow 4P_{3/2}, F' = 9/2$ transition with 10% of the 405 nm beam intensity. Near zero velocity, the damping rate is $\gamma = 1.8 \times 10^4$ s^{-1} for the red and $\gamma = 6.9 \times 10^4$ s^{-1} for the blue. Near zero displacement, the spring constant corresponds to an undamped trap frequency $\omega_{\rm osc}/(2\pi) = 730$ Hz for the red and $\omega_{\rm osc}/(2\pi) = 650$ Hz for the blue.

capture range are greatly reduced. Figure 2(b) shows that the spring constant is comparable for the two transitions, but that trapping volume is larger for the red MOT. These calculations support the strategy of loading atoms using the 767 nm transition and then transferring later to the 405 nm MOT for additional cooling and compression. We find a steady-state temperature of 24 μK for the blue transition, which is indeed smaller than the Doppler temperature of the $D2$ transition. In fact, this steady-state temperature in the low-intensity limit is slightly ($\sim$18%) less than the $\hbar\Gamma/(2k_{\rm B})$ expected in the two-level Doppler cooling, because the multiphoton cascade causes slower momentum diffusion than single-photon kicks with the same total energy.

Another difference between laser cooling with blue instead of infrared light is the possibility of photoionization. The ionization energy of potassium is $h \times 1049.567\,82(2)$ THz [15], so the $5P$ state can be ionized by the 405 nm MOT light, or by any photon with a wavelength less than 972 nm. By contrast, the $4P$ state requires photons with a wavelength less than 455 nm, which is not provided by the $D2$ MOT. The 405 nm trap light may also ionize any state during the radiative cascade, and the 767 nm repump can only ionize the $5P$ state.

III. LASER AND MOT SETUP

The $4S \rightarrow 5P$ transition is in a wavelength band covered by GaN diode lasers, which have become readily available due to recent commercial interest in optical storage media. These sources have been exploited to perform $4S \rightarrow 5P$ spectroscopy of naturally abundant potassium [18,20–23] and enriched ^{40}K [24], and here we use them for laser cooling of enriched ^{40}K.

Our 405 nm master is a grating-stabilized diode laser with 10 mW output. Half of this power is injected [25] into a 100 mW diode laser ("slave" laser). At room temperature and without injection, the slave diode spectrum is nearly 1 nm wide and centered at 407 nm. The poor current and temperature tuning characteristics of the diode, approximately +0.02 nm/mA and +0.05 nm/°C, respectively, necessitate cooling the diode to $-20\,^{\circ}$C. Without injection, the Fabry-Perot spectrum of the slave is featureless, but a single strong peak is evident when successfully injected. The output of the slave, typically run at 60 mW, is passed through a single-mode optical fiber before being used for the MOT (see Fig. 3).

The remaining 5 mW of master light is used for modulation transfer spectroscopy using a natural-abundance potassium cell heated to 140 °C. The elevated temperature is necessary because the absorption of light at the $4S \rightarrow 5P$ resonance by the Doppler-broadened vapor is two orders of magnitude weaker than at the $D2$ transition. We lock to the $4S_{1/2}, F = 1 \rightarrow 5P_{3/2}$ transition in ^{39}K (with unresolved excited states) that is the closest spectral feature to the $4S_{1/2}, F = 9/2 \rightarrow 5P_{3/2}, F' = 11/2$ transition of ^{40}K. The additional 0.5 GHz shift is performed with acousto-optic modulators.

The $D2$ MOT uses retroreflected beams along three axes, limited by the cell windows to be 4.4 cm diameter in the horizontal axes and 3.8 cm diameter in the vertical axis. A background potassium vapor is created from enriched dispensers (5% ^{40}K) and collected in the trap using the strong $4S_{1/2} \rightarrow 4P_{3/2}$ transition. During this phase, there are two overlapping 767 nm beams: a trap with 200 mW total power detuned by $\Delta = -35$ MHz from the $F = 9/2 \rightarrow F' = 11/2$ transition, and a repump with 150 mW total power detuned by -25 MHz from the $F = 7/2 \rightarrow F' = 9/2$ transition. After 10 s, the blue MOT is turned on, with up to 30 mW total power. As shown in Fig. 3, the smaller (10 mm diameter) blue beams are mixed with the infrared beams on dichroic mirrors. There is a short time (3 ms) when both MOTs are on before the $D2$ trap light is turned off (see timing diagram of Fig. 3), while the $D2$ repump beam is left on at reduced intensity. Blue laser cooling is applied typically for 30 ms.

Laser-cooled atoms are characterized using absorption imaging on the $4S \rightarrow 4P$ transition. Temperature is measured after ballistic expansion, with a Gaussian fit to the density distribution imaged at various free-flight times, 1.5–10 ms after the magnetic field and laser beams have been extinguished.

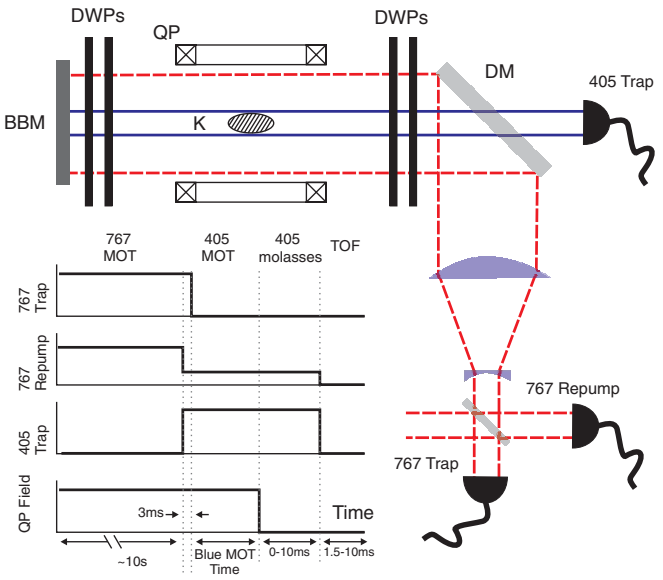

FIG. 3. (Color online) The optical configuration of the magneto-optical trap includes 767 nm trapping and repump beams (both shown with red dashed outlines) and a 405 nm trapping beam (shown in solid blue). The two colors are mixed on a dichroic mirror (DM), manipulated with dichroic quarter-wave plates (DWPs), and retroreflected off a broadband mirror (BBM). Each DWP has a quarter-wave retardation at one wavelength and no retardation at the other wavelength. Only one MOT direction has been shown for clarity, but there is an identical beam path in three orthogonal directions. The magnetic quadrupole (QP) coils typically apply 10 G/cm along their strong axis. The potassium (K) cloud is imaged in absorption with a probe beam (not shown). Inset: Timing diagram of laser beam intensities (top three lines) and magnetic field strength. After a 10 s accumulation, the 767 nm trap is extinguished, the 767 nm repump intensity is reduced, and the 405 nm trap is turned on for a variable hold time. The molasses phase is only used in Sec. V. An absorption image is taken after a variable-length time of flight (TOF).

IV. $4S \rightarrow 5P$ MOT OF ^{40}K

We observe that atoms are held by the blue MOT. A typical absorption image of the $D2$ MOT and the blue MOT are shown in Fig. 4. Compression occurs across a broad range of parameters, which is a first indication of cooling (see below for further discussion). Figure 4(c) shows that cloud sizes in the blue MOT equilibrate with a $1/e$ relaxation time of 2–4 ms. In a damped oscillator model of atomic motion in a MOT, where $\gamma \gg \omega_{\rm osc}$, the atomic position damps with a time $\gamma/\omega_{\rm osc}^2 \sim 4$ ms [using the typical force curves of Fig. 2(b)]—which is comparable to what we measure. Atomic velocities would damp in a much faster time $\gamma^{-1} \sim 15\ \mu$s so, after the spatial compression shown in Fig. 4(c), blue laser cooling is complete.

Figure 5 shows the capture fraction and gravitational sag as a function of blue trap intensity and $D2$ repump intensity. In both cases, providing the saturation intensity (see Table I) is sufficient for complete transfer into a strong trap.[1] From

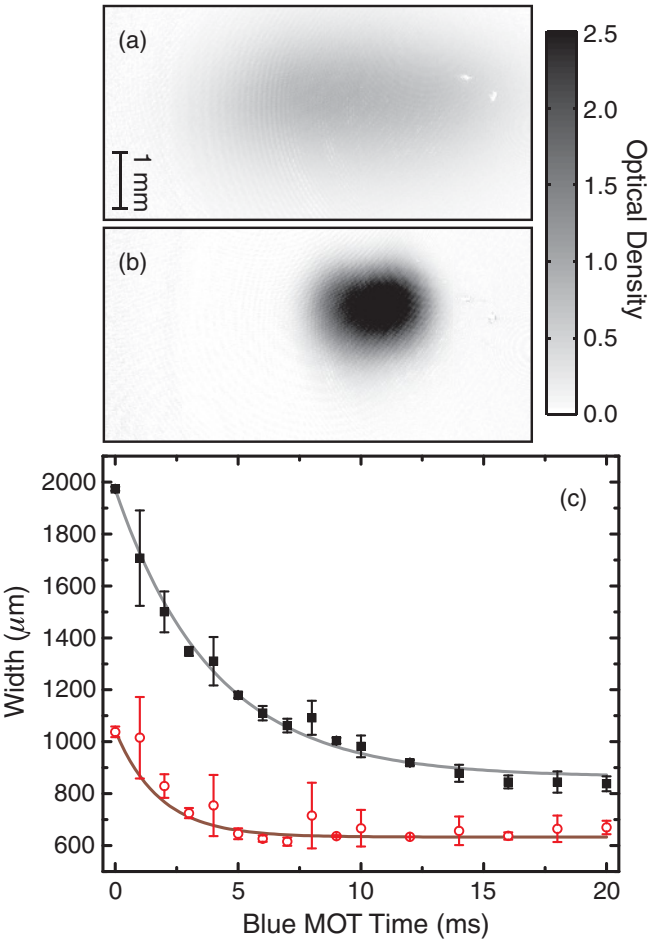

FIG. 4. (Color online) Trapped cloud measurements. Typical absorption images of (a) a 767 nm MOT with detuning $\Delta = -35$ MHz and intensity $I \approx 16$ mW/cm^2 and (b) a 405 nm MOT, for $\Delta = -1$ MHz, $I \approx 90$ mW/cm^2. In both images, pixel darkness denotes optical density. Images were taken shortly (1.5 ms) after release from the trap, such that clouds are little changed from their *in situ* distributions. Atom number is 10^8, but the cloud in (b) is clearly compressed. (c) Cooling dynamics are observed in images similar to (b) but with various hold times in a blue MOT; here with $\Delta = -2$ MHz and $I \approx 50$ mW/cm^2. The rms width is shown for both the vertical (open red circles) and horizontal (black squares) directions. Simple exponential fits are shown as solid lines, with a $1/e$ time of 1.8 ms for the vertical width and 4 ms for the horizontal width.

exponential fits, the transfer efficiency is 90% for 5.5 mW/cm^2 of blue trap intensity and for 0.21 mW/cm^2 of $D2$ repump intensity. The 26:1 ratio between these follows approximately the ratio of saturation intensities of each transition.

Since the capture rate of a MOT from background vapor is proportional to $\Gamma^4 d^4$ for small beam sizes d, one would expect a 10^6 reduction in steady-state number in going from the 767 nm trap to the 405 nm trap. Accordingly, a measurement of

[1]For low intensities, the measured sag values are roughly ten-times larger than the sag one would expect from our simple model. Also note that the displacement switches sign for intermediate repump intensity, which would not be the case if the spring constant were monotonic in intensity. It may be that optical pumping is not correctly functioning in a MOT at intensities far below saturation.

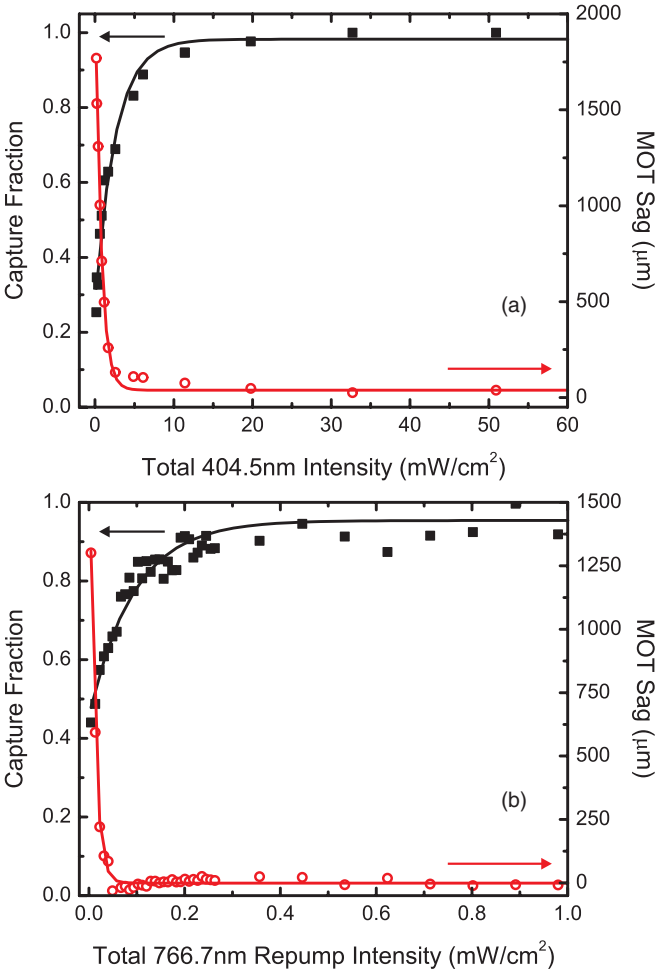

FIG. 5. (Color online) Intensity requirements. A threshold for proper trap function is observed by measuring the capture fraction (black squares, scale on left) and vertical displacement of the cloud from trap center (open red circles, "MOT sag" scale on right) as a function of the six-beam intensity of (a) trap beams and (b) repump beams. Lines are exponential fits to guide the eye. The blue-MOT time was 30 ms for (a) and 20 ms for (b), both at −2 MHz detuning. In both sets of data, the trap movement in the direction orthogonal to gravity was less than 100 μm.

atom number versus time (Fig. 6) shows no sign of saturation after a hundred-fold reduction in number. We can then use such a measurement as a clean measure of loss processes, ignoring additional capture.

We also note that, since we are not loading atoms from vapor into the blue MOT, we can choose small beam sizes and reduce the 405-nm power requirement. In our configuration, the total power required at saturation intensity is roughly 2.5 mW, which our laser system can easily provide.

The loss data in Fig. 6 fit well to two exponential time scales, indicative of two-body losses at high density and one-body losses (collisions with background atoms plus photoionization) at low density. The loss rate from a MOT is [2]

$$\frac{dN}{dt} = -\frac{N}{\tau} - \beta \int n(\vec{r})^2 d^3\vec{r}, \qquad (1)$$

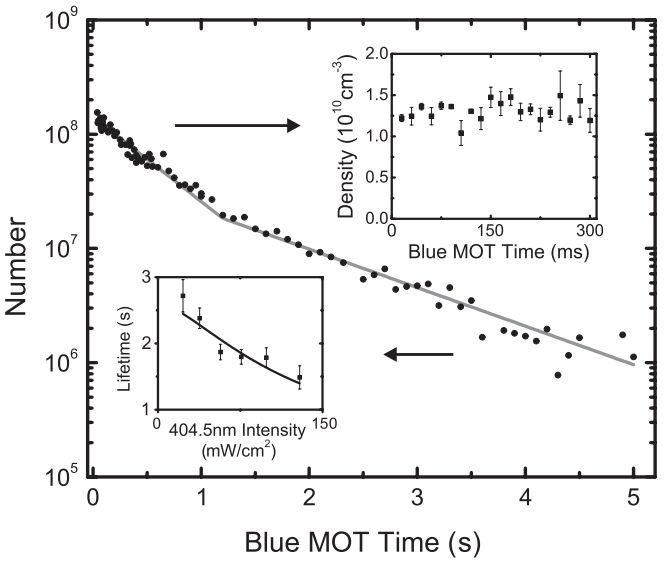

FIG. 6. Lifetime. Atom number is shown versus hold time in the blue MOT. The data are fit to exponential decays in different regions as a guide to the eye. Top inset: Peak density for short hold times is approximately constant. Bottom inset: The one-body-lifetime fit at long hold times decreases at higher 405 nm trap intensity.

where τ is the one-body lifetime, β is the two-body loss coefficient, n is the atomic number density, and the integral is over three-dimensional space. To find τ, we fit the data at long hold times ($t > 2$ s, $N < 5 \times 10^6$) where the atom number is strongly reduced and two-body losses can be neglected. The lifetime versus 405 nm intensity is shown as the bottom inset to Fig. 6. The decrease in lifetime versus intensity could be evidence of ionization losses. The line is a fit to a model that includes the intensity dependence of both the ionization rate and the excited-state fraction. A separate study of MOT fluorescence versus laser power, comparing $D2$ and blue MOTs, was used to calibrate excited state fraction versus intensity. Together, we find an ionization cross section of 8×10^{-18} cm^2 for the $5P_{3/2}$ state at 405 nm. We report this value as an upper bound since the ionizing beams are also the trap beams, and we cannot rule out other trap loss processes.[2]

There are no measured cross sections for the ionization of the $5P$ states of potassium—only for the equivalent state, $6P$, of rubidium [26–28]. These rates may be comparable since the ionization cross section from the potassium $4P$ states [29,30] is within a factor of three of the $5P$ cross section for rubidium [31]. Indeed, our upper bound is similar in magnitude to the 2×10^{-18} cm^2 cross section for the $6P$ state of rubidium from [26] measured at $\lambda = 350$ nm.

To measure the two-body loss rate, we assume the MOT density distribution is Gaussian, which is supported by absorption images of the cloud. From the top inset in Fig. 6 we

[2]From similar measurements of lifetime versus repump intensity, we constrain the effect of repump ionization to be negligible. One would guess a 15 s ionization time for $I_{767} = 1$ mW/cm^2 using the rubidium ionization cross section of $\sigma = 1.5 \times 10^{-17}$ cm^2 measured at 690 nm by [26]

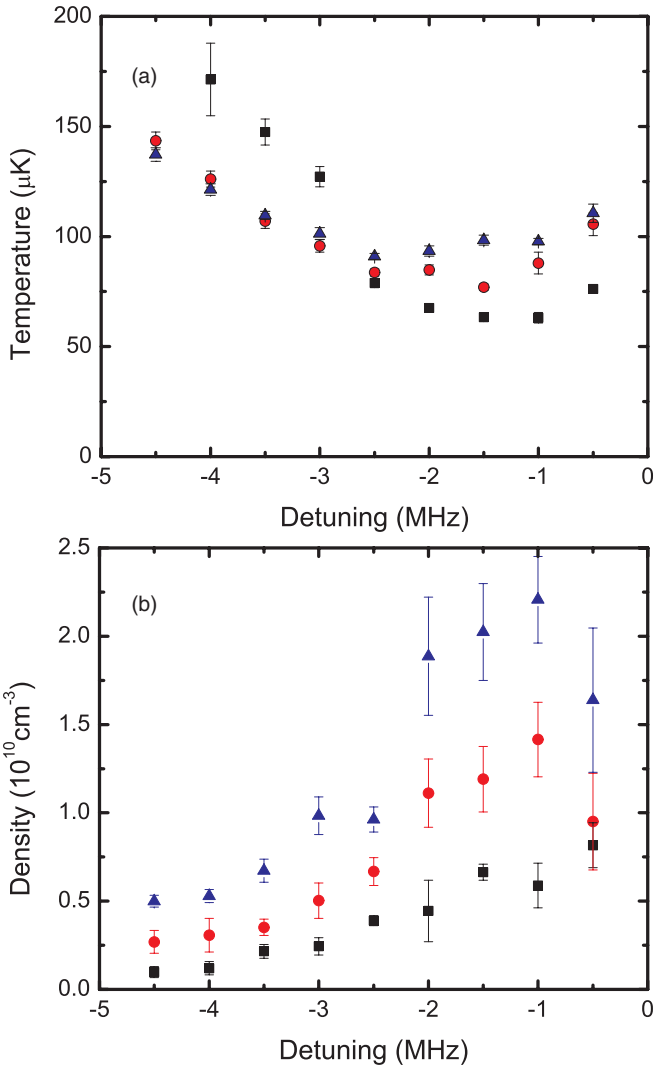

FIG. 7. (Color online) Performance of a magneto-optical trap at 405 nm. Both (a) temperature and (b) peak density are shown versus detuning from resonance, for several magnetic quadrupole gradients: 5 G/cm (black squares), 7.5 G/cm (red circles), and 10 G/cm (blue triangles). Temperature is shown along a weak axis of the quadrupole; temperatures along the strong axis (along gravity) were 1.82(15) times higher.

see that the peak density n_0 at short times is roughly constant, so the number decays as [2]

$$N(t) = N_0 \exp\left[-\left(\frac{1}{\tau} + \frac{n_0\beta}{\sqrt{8}}\right)t\right]. \qquad (2)$$

We then fit the data at short hold times ($t < 300$ ms) to an exponential decay and use τ (from our previous measurement) and n_0 to find β. At $\Delta = -2$ MHz, we find $\beta = 2.0(1) \times 10^{-10}$ cm^3/s for $I \approx 75$ mW/cm^2, and $\beta = 1.4(1) \times 10^{-10}$ cm^3/s for $I \approx 20$ mW/cm^2. These are relatively high two-body loss rates compared to ^{40}K MOTs on the $D2$ transition, which are typically in the range of 10^{-12} to 10^{-10} cm^3/s [32–34]. Therefore, density-dependent loss rates in the potassium nS-$(n+1)P$ MOT, unlike metastable helium [10], are not smaller than in the nS-nP MOT. However, for the short timescales (tens of milliseconds) required to decrease temperatures and increase density, these loss rates are still negligible.

A primary motivation for cooling on a narrow transition is to achieve a lower asymptotic temperature. Figure 7 shows how the temperature and peak density of the blue MOT change with detuning, at various quadrupole gradients. A minimum temperature of 63(6) μK is seen for a 5 G/cm magnetic quadrupole gradient. Operating the MOT with higher gradients increases both the temperature and density. In all cases, the minimum temperature and maximum density are found near $\Delta/\Gamma \approx -1$.

We attribute the increase in density to three factors. First, the temperature in the MOT is lower. Second, expulsive forces due to reabsorption are reduced, because the same spring constant is achieved with a scattering rate that is six times smaller. The open transition may further reduce reabsorption by pumping to the $F = 7/2$ ground states. Third, the optical density seen by both the incident and the scattered blue photons is reduced by a factor of nearly thirty.

In comparison, our $D2$ MOT density is typically $n_0 = 2 \times 10^9$ cm^{-3} and the temperature is typically $T = 180$ μK. Since phase-space density scales as $n_0 T^{-3/2}$, the combined 75 μK and $n_0 = 1.2 \times 10^{10}$ cm^{-3} (achieved with a blue MOT at 7.5 G/cm and -1.5 MHz detuning) realizes a twenty-fold enhancement in phase-space density.

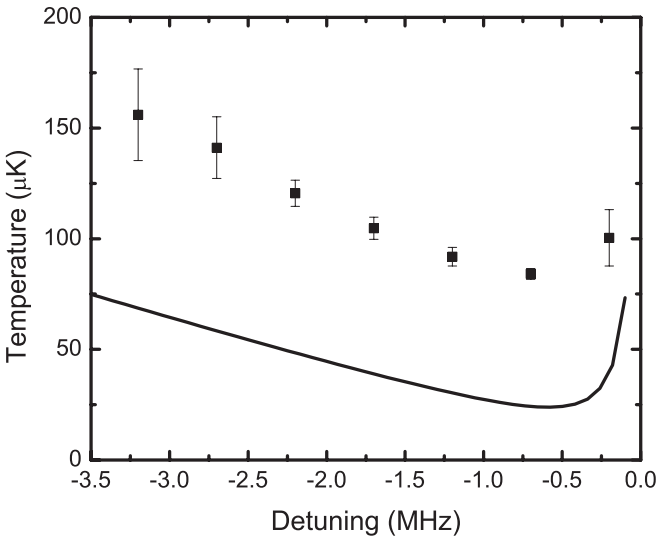

FIG. 8. Molasses cooling. Blue laser cooling is continued for 10 ms after the magnetic quadrupole field is extinguished, followed by a TOF temperature measurement. The horizontal temperature is shown versus detuning; vertical (along gravity) temperatures are 1.96(11) times higher. In addition to the statistical error bars shown, there is a systematic 0.5 MHz uncertainty in the detuning. The solid line is an OBE calculation, but it is not a quantitative prediction: the approach is constrained to intensities well below saturation (here, $I_{sat}/50$ per beam), whereas the data were taken with roughly $I_{sat}/2$ per beam.

V. PROSPECTS AND CONCLUSIONS

Since the lowest observed MOT temperatures occur at low gradients, one might expect continued improvement during an optical molasses phase in which magnetic fields have been extinguished (see Fig. 3 inset). Figure 8 shows that the minimum molasses temperature, roughly 85 μK, is comparable to what is observed in the MOT, although optimized at a lower detuning, $\Delta/\Gamma = -0.6(2)$. These temperatures are still more than three times the Doppler temperature calculated in Sec. II, which may be due to a low cooling rate as compared to the short molasses time available. Indeed, we observe that the temperature asymmetry between the vertical and horizontal axes in the MOT persists during the molasses phase, when no gradient asymmetry remains. Even the asymptotic temperature might not be expected to reach the Doppler limit: while the calculation in Sec. II includes multilevel effects, it neglects three-dimensional effects, reabsorption, and heating due the intensity fluctuations. The latter effect has been shown by Chanelière *et al.* to limit one-dimensional Doppler cooling to several times T_D in Sr, when Sisyphus and other sub-Doppler mechanisms are absent [35]. In the case of $4S \rightarrow 5P$ cooling in ^{40}K, polarization gradient cooling may be interrupted by the optical pumping and depolarization effects of the three-photon cascade.

We have also observed laser cooling and trapping for bosonic ^{41}K on the $4S_{1/2} \rightarrow 5P_{3/2}$ transition. A similar order-of-magnitude increase in MOT density was apparent, although further study is warranted. With any isotope of potassium, additional improvements might be possible with more sophisticated timing sequences of detuning and/or intensity of cooling light, which has been fruitful in narrow-line MOTs and in sub-Doppler cooling of bosonic potassium [36].

The reduced wavelength of the $4S_{1/2} \rightarrow 5P_{3/2}$ transition may enable improved imaging or addressing resolution, for instance in the context of strongly correlated lattices where the spacing is typically 0.5 μm [37]. However ionization will eventually limit the number of photons that can be scattered from an atom, and thus the fidelity of imaging. Using an objective with 0.6 numerical aperture, collection efficiency would be 10% and resolution would be 0.4 μm. In such a configuration, our results suggest that fluorescence imaging at $I_{sat}/4$ could collect 10^4 blue photons with a 1% upper bound on the probability of ionization. Lowering the imaging beam intensity would lower the ionization probability for the same number of collected photons, but would require longer imaging times.

In sum, we have observed laser cooling and trapping of neutral potassium on the open $4S_{1/2} \rightarrow 5P_{3/2}$ transition. Nearly complete transfer from a $D2$ MOT is observed, although the blue MOT is ineffective at capturing directly from the vapor. We observe temperatures as low as 63(6) μK along one axis, roughly half of the Doppler limit on the $D2$ transition. Unlike sub-Doppler cooling observed in ^{40}K during a molasses phase [7], our approach reduces temperature while the confining MOT quadrupole field is still present. Density is enhanced tenfold in typical conditions, due to lower temperature and reduced reabsorption effects. Cooling and compression together increase the phase-space density by more than an order of magnitude, demonstrating improved precooling for quantum degenerate gas experiments. More generally, since the potassium cascade structure is shared by sodium, rubidium, cesium, and francium, our work along with Ref. [13] suggests that laser cooling and trapping using the $nS \rightarrow (n+1)P$ transition will be successful for all alkali metals.

ACKNOWLEDGMENTS

We thank K. Pilch, M. Schöll, and F. Stubenrauch for their early contributions, and B. DeMarco, P. Duarte, M. Greiner, E. Hessels, R. Hulet, A. Steinberg, S. Trotzky, and D. Weiss for discussions. This work was supported by the DARPA OLE program, ARO, AFOSR, CIfAR, CFI, and NSERC.

[1] T. Walker, D. Sesko, and C. Wieman, Phys. Rev. Lett. **64**, 408 (1990); K. Lindquist, M. Stephens, and C. Wieman, Phys. Rev. A **46**, 4082 (1992).

[2] J. Weiner, V. S. Bagnato, S. Zilio, and P. S. Julienne, Rev. Mod. Phys. **71**, 1 (1999).

[3] D. J. Wineland and W. M. Itano, Phys. Rev. A **20**, 1521 (1979); V. S. Letokhov and V. G. Minogin, Phys. Rep. **73**, 1 (1981); A. Ashkin and J. P. Gordon, Opt. Lett. **4**, 161 (1979).

[4] P. Lett, W. Phillips, S. Rolston, C. Tanner, R. Watts, and C. Westbrook, J. Opt. Soc. Am. B **6**, 2084 (1989).

[5] J. Dalibard and C. Cohen-Tannoudji, J. Opt. Soc. Am. B **6**, 2023 (1989).

[6] Z. Lin, K. Shimizu, M. Zhan, F. Shimizu, and H. Takuma, Jpn. J. Appl. Phys. **30**, L1324 (1991).

[7] G. Modugno, C. Benkő, P. Hannaford, G. Roati, and M. Inguscio, Phys. Rev. A **60**, R3373 (1999); F. S. Cataliotti, E. A. Cornell, C. Fort, M. Inguscio, F. Marin, M. Prevedelli, L. Ricci, and G. M. Tino, *ibid.* **57**, 1136 (1998).

[8] B. DeMarco and D. S. Jin, Science **285**, 1703 (1999).

[9] K. Vogel, T. Dinneen, A. Gallagher, and J. Hall, IEEE Trans. Instrum. Meas. **48**, 618 (1999); H. Katori, T. Ido, Y. Isoya, and M. Kuwata-Gonokami, Phys. Rev. Lett. **82**, 1116 (1999).

[10] J. C. J. Koelemeij, R. J. W. Stas, W. Hogervorst, and W. Vassen, Phys. Rev. A **67**, 053406 (2003); A. S. Tychkov, J. C. J. Koelemeij, T. Jeltes, W. Hogervorst, and W. Vassen, *ibid.* **69**, 055401 (2004).

[11] J. J. McClelland and J. L. Hanssen, Phys. Rev. Lett. **96**, 143005 (2006).

[12] S. Wu, T. Plisson, R. C. Brown, W. D. Phillips, and J. V. Porto, Phys. Rev. Lett. **103**, 173003 (2009).

[13] P. M. Duarte, R. A. Hart, J. M. Hitchcock, T. A. Corcovilos, T.-L. Yang, A. Reed, and R. G. Hulet, Phys. Rev. A **84**, 061406 (2011).

[14] E. S. Shuman, J. F. Barry, and D. DeMille, Nature **467**, 820 (2010).

[15] J. E. Sansonetti, J. Phys. Chem. Ref. Data **37**, 7 (2008).

[16] H. Wang, J. Li, X. T. Wang, C. J. Williams, P. L. Gould, and W. C. Stwalley, Phys. Rev. A **55**, R1569 (1997).

[17] R. Berends, W. Kedzierski, J. Atkinson, and L. Krause, Spectrochim. Acta, Part B **43**, 1069 (1988).
[18] A. Mills, J. A. Behr, L. A. Courneyea, and M. R. Pearson, Phys. Rev. A **72**, 024501 (2005).
[19] E. Arimondo, M. Inguscio, and P. Violino, Rev. Mod. Phys. **49**, 31 (1977).
[20] U. Gustafsson, J. Alnis, and S. Svanberg, Am. J. Phys. **68**, 660 (2000).
[21] U. Gustafsson, G. Somesfalean, J. Alnis, and S. Svanberg, Appl. Opt. **39**, 3774 (2000).
[22] S. Uetake, K. Hayasaka, and M. Watanabe, Jpn. J. Appl. Phys. **42**, L332 (2003).
[23] L. Halloran, S. Fostner, E. Paradis, and J. Behr, Opt. Commun. **282**, 554 (2009).
[24] A. Behrle, M. Koschorreck, and M. Köhl, Phys. Rev. A **83**, 052507 (2011).
[25] C. Y. Park and T. H. Yoon, Jpn. J. Appl. Phys. **42**, L754 (2003); K. Komori, Y. Takasu, M. Kumakura, Y. Takahashi, and T. Yabuzaki, *ibid.* **42**, 5059 (2003).
[26] R. V. Ambartzumian, N. P. Furzikov, V. S. Letokhov, and A. A. Puretsky, Appl. Phys. **9**, 335 (1976).
[27] M. Anderlini, E. Courtade, D. Ciampinie, J. H. Müller, O. Morsch, and E. Arimondo, J. Opt. Soc. Am. B **21**, 480 (2004).
[28] E. Courtade, M. Anderlini, D. Ciampini, J. H. Müller, O. Morsch, E. Arimondo, M. Aymar, and E. J. Robinson, J. Phys. B **37**, 967 (2004).
[29] I. Petrov, V. Sukhorukov, E. Leber, and H. Hotop, Eur. Phys. J. D **10**, 53 (2000).
[30] N. Amina, S. Mahmooda, S. Haqa, M. Kalyara, M. Rafiqa, and M. Baig, J. Quant. Spectrosc. Radiat. Transfer **109**, 863 (2008).
[31] T. P. Dinneen, C. D. Wallace, K.-Y. N. Tan, and P. L. Gould, Opt. Lett. **17**, 1706 (1992).
[32] G. Modugno, G. Roati, M. Inguscio, M. Santos, G. Telles, L. Marcass, and V. Bagnato, Eur. Phys. J. D **23**, 409 (2003).
[33] T. Tiecke, Ph.D. thesis, University of Amsterdam, 2009 (unpublished).
[34] A. Ridinger, S. Chaudhuri, T. Salez, U. Eismann, D. R. Fernandes, K. Magalhães, D. Wilkowski, C. Salomon, and F. Chevy, Eur. Phys. J. D **65**, 223 (2011).
[35] T. Chanelière, J.-L. Meunier, R. Kaiser, C. Miniatura, and D. Wilkowski, J. Opt. Soc. Am. B **22**, 1819 (2005).
[36] M. Landini, S. Roy, L. Carcagní, D. Trypogeorgos, M. Fattori, M. Inguscio, and G. Modugno, Phys. Rev. A **84**, 043432 (2011).
[37] W. S. Bakr, J. I. Gillen, A. Peng, S. Fölling, and M. Greiner, Nature (London) **462**, 74 (2009); J. F. Sherson, C. Weitenberg, M. Endres, M. Cheneau, I. Bloch, and S. Kuhr, *ibid.* **467**, 68 (2010).